# Post-Synthetic Annealing: Linker Self-Exchange in UiO-66 and its Effect on Polymer-MOF Interaction

*Stefan J. D. Smith,* † ‡ Kristina Konstas† Cher Hon Lau,†§ Yesim M. Gozukara,† Christopher D. Easton,† Roger J. Mulder,† Bradley P. Ladewig, ‡• and Matthew R. Hill*† ‡*

† Manufacturing, CSIRO, Clayton, 3168, Australia

‡ Department of Chemical Engineering, Monash University Clayton, VIC 3800, Australia.

§ Department of Chemical Engineering, The University of Edinburgh, Edinburgh EH9 3JL, United Kingdom

• Barrer Centre, Department of Chemical Engineering, Imperial College London, Exhibition Road, London SW7 2AZ, United Kingdom

KEYWORDS

Metal-organic frameworks, Post-synthetic modification, Nanocomposite, Membranes

ABSTRACT

Post-Synthetic Exchange (PSE) and Defect Engineering have emerged as powerful techniques for tuning the properties and introducing novel functionality to Metal Organic Frameworks (MOFs). Growing evidence suggests that each technique plays a key role in the mechanism of the other: linker coordination chemistry is pivotal to defective frameworks, while defect sites can help initiate PSE. Here, the intersection of these approaches is explored by exchanging a MOF with linkers already present within the framework. Post-Synthetic Annealing (PSA) modifies a MOF's properties by redistributing the framework's mixture of bound linker/modulator species. Using changes to the polymer-additive interactions in PTMSP (poly-1-trimethylsilyl-1-propyne) nanocomposites observed through aging, we demonstrate that PSA causes one linker species to preferentially accumulate on the MOF's crystal surface. Reaction conditions are shown to affect molecular composition of the resulting annealed UiO-66 MOFs; a finding explained through established reaction constants. This work simultaneously reveals intricacies of Post-Synthetic Modification (PSM) chemistry and presents a facile means of tuning MOFs and MOF nanocomposites.

INTRODUCTION

Metal Organic Frameworks (MOFs) have emerged as an exciting class of materials for numerous applications due to the near-infinite tunability of their highly porous lattice structures.[1-9] Recently, Cohen[10] reviewed the chemistry of Post-Synthetic Modifications (PSM), based upon the deliberate exchange or modification of linkers and/or metal centers in MOFs.[11-13] Categorically, PSM groups together a range of techniques including: Post-Synthetic Exchange (PSE)[14-16] or Solvent Assisted Linker Exchange (SALE),[17-18] cluster metalation,[19-21] and linker

functionalization,[8, 17, 22-26] among others; many of which have been reported to improve the performance of MOFs as adsorbents,[15, 27] catalysts,[19-21, 28-29] and as additives in Mixed Matrix Membranes (MMM).[30-33] Critically, PSM mechanisms occur without complete dissolution and recrystallization of the parent MOF enabling preparation of MOF structures that are not possible by direct synthesis methodologies.[14, 34-35] Here we add Post-Synthetic Annealing (PSA) to the list of PSM techniques (**Figure 1**). PSA differs from other methods as no reagent is added to modify or exchange the framework; instead linkers already present in the framework exchange with one another to alter the MOF's properties. This differs from the previous use of the term "Post-synthesis Annealing" that described the partial thermal decomposition of MOF-5,[36] a process more akin to a partial carbonization of the MOF than the structural rearrangement presented here.[9, 37]

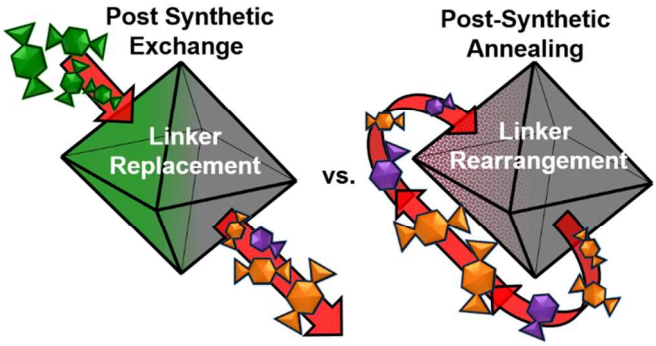


**Figure 1.** General scheme showing how Post-Synthetic Annealing differs from Post-Synthetic Exchange and other Post-Synthetic Modifications.[10]

Many works propose mechanisms for metal and linker exchange reactions,[16] however characterization of MOFs at the molecular level is generally difficult, limiting our understanding of the steric and electronic factors behind MOF coordination chemistry.[16, 38-39] For example,

Nguyen *et. al.*[20] compared the properties of titanium modified UiO-66 *via* Ti exchange and addition to the $Zr_6O_6$ secondary building unit (SBU), showing that a minor change to the $Ti^{IV}$ reagent used resulted in considerably different hetereometallic Ti-UiO-66 MOFs. A shortfall in many PSM works is that modified MOFs are generally characterized from the perspective that the parent and product MOF are comprised of 'ideal' unit cells. Little consideration is given for how modulator species, defects, and distribution of these features affect the PSM chemistry.[16, 40] Defect Engineering - the intentional introduction of defects into a framework - has emerged as a separate route of controlling MOF properties.[40-42] Structural defects occur naturally in a few MOFs, including HKUST-1,[43] MOF-5,[44] and UiO-66;[45] however heterogeneity can also be introduced *via* tuning synthesis conditions and the inclusion of non-bridging linkers or modulator species, such as acetic acid, formic acid, or benzoic acid.[15, 30, 46-48] During synthesis, modulators reversibly bind to the forming MOF's metal cluster nodes, or SBU, effectively controlling crystal growth and directing missing linker defects in the MOF.[46, 48-50] Recently, Hu *et. al.*[51] examined the effect of modulator chemistry on the properties of Zr/Hf MOFs, finding that modulator/linker acidity strongly influenced defect concentration, pore size, surface area and other MOF properties. Yaghi and co-workers[52] prepared large (300 μm) single UiO-66 crystals using an optimized synthesis method, importantly confirming that coordinating modulator species are retained within the washed MOF (balancing charge on defect metal sites) and are only replaced by hydroxide anions after high temperature activation.[47-48] Similarly, Vermoortele *et. al.* showed that trifluoroacetate is removed from UiO-66 during activation at 320°C; exposing the framework's metal sites and greatly enhancing the MOF's catalytic activity.[53]

We hypothesize that given the equilibrium nature of Post-Synthetic Exchange, linker/modulator chemistry not only influences the synthesis of defective frameworks, but also

plays a key role in the Post-Synthetic Modifications of MOFs.[14, 38-39] In this article, we report the Post-Synthetic Exchange of linkers in a modulated UiO-66 with and without the introduction of "exchangeable" reagents. Characterization of the resulting UiO-66 based MOFs; $PSA_x$UiO-66 (where 'x' describes the PSM period in days) are compared against two transmetalated UiO-66 MOFs ($Ti_5$UiO-66,[15, 20, 30, 32] and its $Zr^{IV}$ equivalent; $Zr_5$UiO-66) to reveal changes to the composition and distribution of coordinated species within the UiO-66. During solvent-only modification to form $PSA_x$UiO-66, UiO-66's labile terephthalic and benzoate linker species are shown to 'self-exchange' resulting in a benzoate-rich crystal surface. Conversely, benzoate is nearly entirely removed from the two transmetalated UiO-66 controls. These changes are confirmed by monitoring physical aging of MOF-loaded poly-1-trimethylsilyl-1-propyne (PTMSP) films; a particularly sensitive technique for detecting changes to additive surfaces by differences in their polymer interaction.[32, 54] $PSA_x$UiO-66's benzoate-rich surface reversed UiO-66's usual incompatibly with the hydrophilic polymer and reduced membrane aging; an approach that may hold considerable value for tuning the 'compatibility' of other MOF-based MMM.[6-7, 55-56] Observed solvent equilibria effects can be explained by the chemistry of terephthalate and benzoate species, in terms of established reactivity constants for benzoic acid derivatives. To the best of our knowledge, this is the first work to demonstrate a non-random linker self-exchange in a metal organic framework, a process we term Post-Synthetic Annealing (PSA).

## RESULTS AND DISCUSSION

UiO-66 was prepared according to the schemes reported previously using a benzoic acid modulators in the precence of $H_2O$.[15, 30, 32] After washing, UiO-66 was activated at 120°C under vacuum overnight. Although generally considered a modulator during MOF synthesis, benzoate

is refered herein as a (non-bridging) linker for the discussion of Post-Synthetic Modifications. Post-Synthetic Exchange was undertaken in DMF (20 mL/g UiO-66) with an equimolar quantity of $TiCl_4(THF)_2$ or $ZrCl_4$ (where applicable) at 90°C for 5 or 15 days, according to our previous works (**Table S1**).[15, 30, 32] To maintain processing history, each of the exchanged MOFs, and the precursor UiO-66 were re-washed and activated. As with previous reports, UiO-66's crystal structure integrity was retained during each of the PSM reactions (**Figure S1i**).[14-15, 20, 30, 32] Diffraction patterns for the $PSA_x$UiO-66 appeared identical to UiO-66, while some peak broadening was observed for the heterometallic $Ti_5$UiO-66, whereas the $Zr_5$UiO-66 pattern appeared sharper.[20, 28, 30] Although lower than our previous works,[15, 30] the Brunauer-Emmett-Teller (BET) surface area of the native UiO-66 (851 $m^2/g$) agrees with the range reported in literature for the UiO-66 MOF.[57-58] The Ti and Zr exchanged UiO-66 MOFs displayed higher BET surface areas (1011 $m^2/g$ and 965 $m^2/g$, respectively) than that of the 'solvent-only' exchanged MOFs, which had surface areas in the range of 800-900 $m^2/g$ (**Table S2**). The negligible change of UiO-66's surface area after PSA suggests the process has a minimal effect on overall linker defect concentration within the MOF.[59] While Ti exchanged UiO-66's relatively high surface area has been reported previously,[15] the similar enhancement for $Zr_5$UiO-66 suggests that excess metal ions in solution have a considerable effect on the framework as there is no driving force for introduced $Zr^{IV}$ to exchange with those present in UiO-66 SBU.

FTIR spectra normalized to the symmetric carboxylate vibration ($V_{sym}COO$, 1391 $cm^{-1}$) allows the composition of UiO-66 MOFs to be compared by the relative intensity of carboxylate coordination bonds within their unit cells. Consequently, changes to the molecular composition of UiO-66 linkers during PSM are readily identified by terephthalate and benzoate's unique absorptions at 744 $cm^{-1}$ and 717 $cm^{-1}$, respectively. These assignments are confirmed by

comparison against prior reports of modulated UiO-66 MOFs.[46-47] Using this comparison, **Figure 2i** confirms benzoate concentration is reduced in UiO-66 with increasing degrees of exchange, with no peak observed for either of the two metal exchanged MOFs, $Zr_5$UiO-66 and $Ti_5$UiO-66. Carboxylate absorption peaks ($V_{sym}COO$ and $V_{asym}COO$) are noticeably sharper with increasing exchange as a consequence of the higher purity of terephthalate linkers within the framework, especially after exchange with $TiCl_4$ or $ZrCl_4$ (**Figure 2ii**). Unfortunately, due to the similarity of the environments of carbon in benzoate and terephthalate, solid state $^{13}C$ NMR was unable to confirm the difference in linker composition between UiO-66, $Ti_5$UiO-66 and $PSA_5$UiO-66, though indicated the presence of DMF in each MOF, even after washing (**Figure S2**).

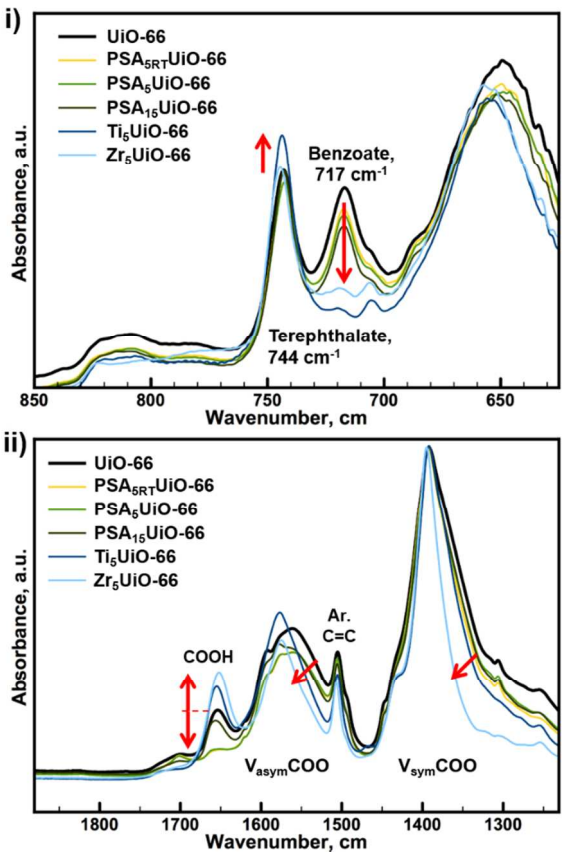

**Figure 2.** Changes to infrared adsorption spectra across the **i)** 600 - 850 $cm^{-1}$ and **ii)** 1200 - 1850 $cm^{-1}$ regions in each of the studied UiO-66 based MOFs, normalised to the peak height of $V_{sym}COO$, 1391 $cm^{-1}$.

The 1650 $cm^{-1}$ (COOH) peak represents singly coordinated (i.e. non-bridging) terephthalic acid present either on the exterior crystal surface or near defects within the framework.[40, 48] Interestingly, non-bridging terephthalate linkers are more prevalent in the metal exchanged MOFs, but almost completely absent in $PSA_{5RT}$UiO-66 and $PSA_5$UiO-66. Unlike Ti/Zr transmetalation which reduces linker bridging, solvent-only PSA appears to result in MOFs free from any non- bridging terephthalate linkers, either by the specific removal of terephthalate linkers with free carboxylic groups, or through the rearrangement of these singly bound species to missing (bridging) linker sites within the framework. $PSA_{15}$UiO-66's increase in free COOH and higher N content are instead attributed to a slight degradation of the framework, though markedly less than previously observed for 15 day titanium exchanged UiO-66.[30] Deconvolution of IR adsorption between 1450 $cm^{-1}$ and 1700 $cm^{-1}$ identifies a number of contributing peaks, however due to the potential mixture of Zr/Ti, different carboxylic species and their potential bonding modes, direct assessment of linker bonding in UiO-66 and $Ti_5$UiO-66 is not possible by the wavenumber difference described by Sabo and co-workers.[60] Instead, we examined the bonding mix through changes to ratio of the terephthalate (744 $cm^{-1}$) and $V_{Sym}COO$ peaks (**Figure S3**). Given the similarity of the 1394 $cm^{-1}$ peak height and starkly different benzoate content in UiO-66 and $Zr_5$UiO-66, we can conclude that benzoate contributes to the broadness of the $V_{sym}COO$ peak, but not its height. Thus, the small reduction of 1394 $cm^{-1}$ absorption in $Ti_5$UiO-66 can be attributed to a reduction in the bidentate coordination of terephthalate in the

MOF, representative of a partial shift to monodentate bonding. This conclusion is supported by Nguyen *et. al.*,[20] who discussed the necessity of post-synthetic methods in the preparation of Ti-exchanged UiO-66 due to Ti's maximum coordination number (6) as being less than that required from each Zr in UiO-66 (7 or 8). For a given number of missing linkers, less exposed metal sites are present in $Ti_5$UiO-66 than $Zr_5$UiO-66, which explains the characterized differences observed between these MOFs. Following this explanation, $PSA_5$UiO-66 and $PSA_{5RT}$UiO-66 appear to exhibit a slight increase in bidentate coordination, which combined with a reduction in free COOH (1650 $cm^{-1}$), indicates that non-bridging terephthalate are annealed to occupy missing linker sites within the framework during exchange.[14]

Small-Angle X-ray Scattering (SAXS) reveals nanometer heterogeneity in the structural density of samples, such as the free volume in polymers or pore size in MOFs. SAXS patterns of the modified MOFs showed a slight broadening and variation of peak intensities, indicative of more defective structures (**Figure 3i**).[32, 40, 48] The small reduction in the size of scattering elements observed in the modified MOFs corresponds to a reduction of the MOF's unit cell size, a trend also seen in the calculated lattice parameters from PXRD. By both of these methods, $Ti_5$UiO-66 exhibited the largest reduction in unit cell size at 0.3 % (**Figure 3i** and **Table S3**).[15]

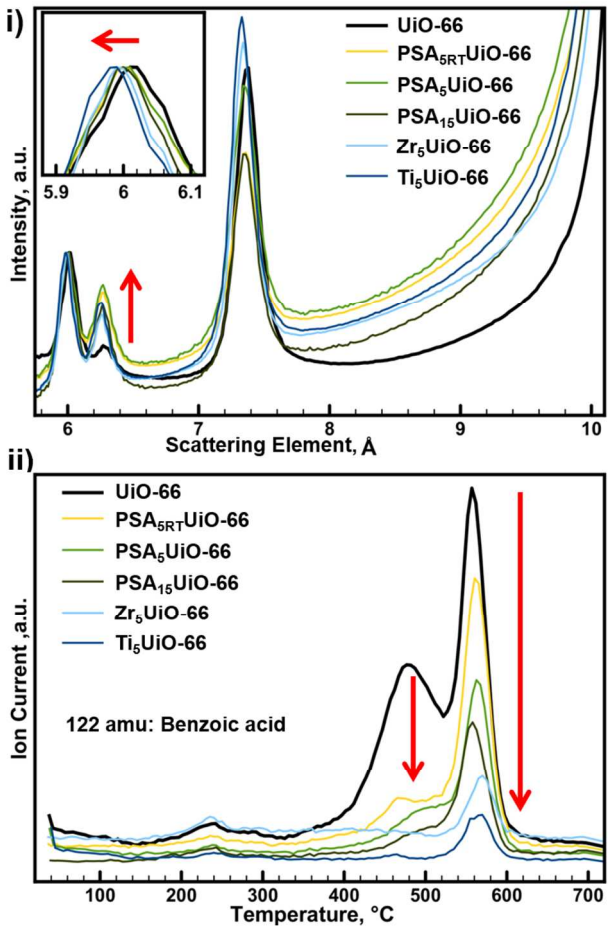


**Figure 3. i)** Small Angle X-ray Scattering patterns, normalized to the ~6 Å peak after subtracting a Kapton background. Red arrows highlight changes to the scattering pattern after PSA or PSE of UiO-66. Insert highlights the discussed reduction in size of scattering elements. **ii)** Mass Spectrometer response from gases evolved during Thermal Gravimetric Analysis of UiO-66 and the exchanged MOFs at 122 amu, associated to benzoic acid/benzoate species. Detected benzoic acid in $Ti_5$UiO-66 and $Zr_5$UiO-66 are explained by the high temperature decomposition of terephthalic acid present in the frameworks. EGA curves for species with masses of 166 amu (terephthalic acid), 78 amu (benzene), and 44 amu (carbon dioxide) are included in the Supporting Information.

Detected elemental composition of the MOFs also changed after both post-synthetic modification methods. Relative to carbon; zirconium, oxygen, and trace nitrogen all increase with longer annealing periods and/or metal exchange (**Table S4**). The $Zr_5$UiO-66 and $Ti_5$UiO-66 display similar Zr/C and O/C ratios; suggesting that metal 'exchange' has a similar effect independent of the metal used. Only nitrogen content, associated to DMF-metal site adducts,[49] separates the two metal-exchanged MOFs. Although not detected by XPS, ICP-OES of the digested MOF confirmed Ti was present in $Ti_5$UiO-66 (**Table S5**). Peak decomposition temperatures under $N_2$ were consistent for each of the studied UiO-66 MOFs (550 ± 5°C), supporting the conclusion that the overall MOF structure was retained. Each of the UiO-66 MOFs exhibited four distinct steps in mass loss during TGA, assigned to the loss of moisture (~100°C), removal/decomposition of guest species (180°C and 230°C), and decomposition of the MOF structure (550°C), respectively (**Figure S5**).[49, 52] Based on the detected masses of decomposition products and the N content of the MOFs , we attribute the ~230°C step to decomposition of DMF present within the structure. Although oxidative conditions are needed for a quantitative $ZrO_2$ residue and missing linker calculation,[59] TGA under inert conditions enables the chemically similar benzoate and terephthalate linkers to be differentiated by Evolved Gas Analysis (EGA). Mass spectrometry of the gases evolved during TGA show a clear reduction in the detected concentration of both linker species (terephthalate, benzoate) and their primary degradation products (benzoic acid, benzene and $CO_2$) in the modified MOFs, increasing with PSM temperature, reaction period, and inclusion of metal ions (**Figure 3ii** and **Figure S6**). Although occurring here at a much higher temperature than Yaghi *et. al.* reported for Zr-bound propoxide in UiO-66 (150-300°C),[52] the peak centered at 480°C in UiO-66 confirms that benzoate is strongly bound to the framework as a counter-ion. This peak is largely absent in each

of the transmetalated and annealed MOFs, indicating that coordinated benzoate is removed during solvent exchange. Unlike other examples of modulated UiO-66,[52-53, 59] coordinated benzoate is not removed from the framework at a sufficiently low temperature that it can be distinguished from the mass loss associated to decomposition. Adapting the protocol by Lamberti and co-workers,[49] the native UiO-66 was estimated to have 9.1 linkers (2.9 missing linkers) per unit cell. The annealed MOFs ($PSA_5$UiO-66, $PSA_{5RT}$UiO-66, and $PSA_{15}$UiO-66) had linker concentrations within experimental error of UiO-66 (9.1 ± 0.03), whereas the metal exchanged $Ti_5$UiO-66 and $Zr_5$UiO-66 had more missing linker defects at 8.36 and 8.15 linkers, respectively (**Table S6**). Of the modified MOFs, only $Zr_5$UiO-66 displayed faster mass loss and had a higher MS response for $CO_2$, benzene and benzoate below 300°C, trends indicative of accelerated linker fragmentation (**Figures S5 and S6**). The low temperature removal and decomposition of linker species in $Zr_5$UiO-66 is a possible consequence of MOF's higher N content (associated to bound DMF), which may generate radicals at elevated temperature. These techniques show that in the absence of an 'exchangeable' linker species or metal ions in solution, Post-Synthetic Annealing has only minor effects on the crystallinity and overall linker composition of UiO-66.

**Polymer Interaction: PSAxUiO-66 in PTMSP Membranes.** In our previous works, surface chemistry of additive materials are shown to greatly affect the performance and aging of polymer membranes.[32, 61-63] Here, we use these methods to confirm the proposed rearrangement of UiO-66 linker species by changes to the polymer interaction with the MOF crystal surface. As expected, the properties of PTMSP nanocomposite membranes varied significantly with each of the studied MOFs. Incorporation of $Ti_5$UiO-66 and UiO-66 further enhanced the gas transport of

PTMSP, whereas the $PSA_xUiO$-66 MOFs either had negative or negligible effects on the gas permeability of PTMSP (**Figure 4**). None of the studied MOFs had a significant effect on the polymer's ideal gas selectivities (**Table S7**).

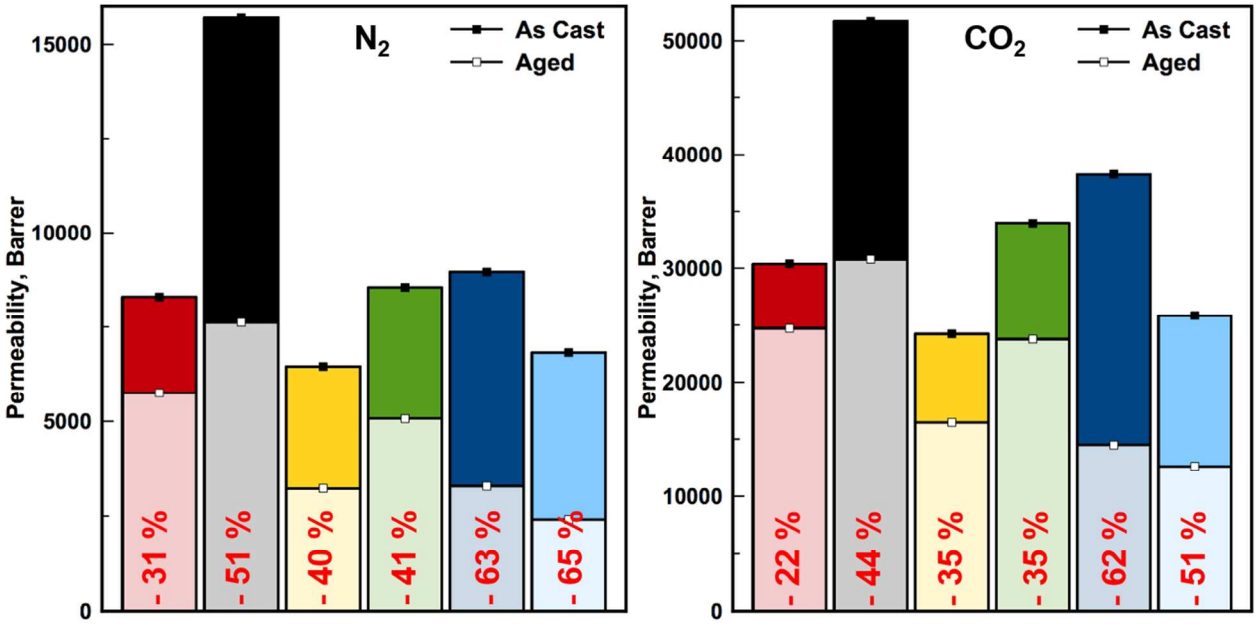


**Figure 4.** Changes in $N_2$ and $CO_2$ permeability of studied UiO-66 MOFs in PTMSP over time. Samples identified by colour: PTMSP (red), PTMSP nanocomposites with UiO-66 (black), $PSA_{5RT}UiO$-66 (yellow), $PSA_5UiO$-66 (green), $Ti_5UiO$-66 (navy), and $Zr_5UiO$-66 (blue). Films aged for 17 days in ambient conditions. Similar trends are observed for the permeability of $H_2$, see **Figure S7** of the Supporting Information.

The opposing effects of $Ti_5/Zr_5UiO$-66 and $PSA_{5/5RT}UiO$-66 in PTMSP are further highlighted in aged films. $Ti_5UiO$-66 and $Zr_5UiO$-66 displayed even greater permeability losses than UiO-66 in PTMSP over time, whereas the $PSA_{5RT}UiO$-66 and $PSA_5UiO$-66 nanocomposites exhibited losses with aging similar to that of the pure polymer. This shift represents a change in the polymer-MOF interface interaction, from repulsion that causes interfacial free volume and localized accelerated aging, to a strong attraction that fixes the polymer chains in place.[32]

The change between these interface types with annealed MOFs was confirmed using SAXS, specifically by the additional peak in the scattering patterns of the faster aging nanocomposites, but not in those prepared with $PSA_{5/5RT/15}$UiO-66 (**Figure 5i**). Similarly, NMR T1 relaxation rate constants depict the change in mobility of carbon in PTMSP with aging. Over time, densification of polymer chains brings the chains closer together, reducing the mobility of individual carbons. PTMSP's tri-methyl-silyl alkene carbon (carbon b) becomes more mobile with age, likely as an effect of the bulky group's steric effects on chain packing.[64] The mobility loss associated with aging was considerably less when $PSA_5$UiO-66 is incorporated in PTMSP nanocomposites, compared to UiO-66, $Ti_5$UiO-66. This demonstrates that Post-Synthetic Annealing strengthens the polymer's adhesive interaction with the MOF surface in a way that reduces polymer chain densification (**Figure 5ii**).[32]

We attribute these observed changes in nanocomposite properties to differences in the $CH_3$- π interaction, between the polymer's pendant methyl groups and the π face of aromatic linkers, at the PTMSP-MOF interface (**Figure 5iii**). Analogous to a 'cup and ball' joint, the benzoate rich MOF surface forms an open pore enabling $CH_3$- π interaction with PTMSP's trimethylsilyl groups.[61] However for the terephthalate decorated MOFs, the hydrophobic polymer's interaction is prevented by its repulsion to the exposed hydrophilic carboxylic acid groups, depicted as red arrows in **Figure 5iii.** Similar behavior is observed from interactions between PTMSP's methyl groups and the exposed benzene/biphenyl groups of other additives, the mechanism credited for PAF-1 and p-DCX's ability to stop physical aging in the glassy polymers.[54, 63] Similarly, chemical and steric functionalization of these aromatic additives also reduced their anti-aging

effect in PTMSP.[61-63]

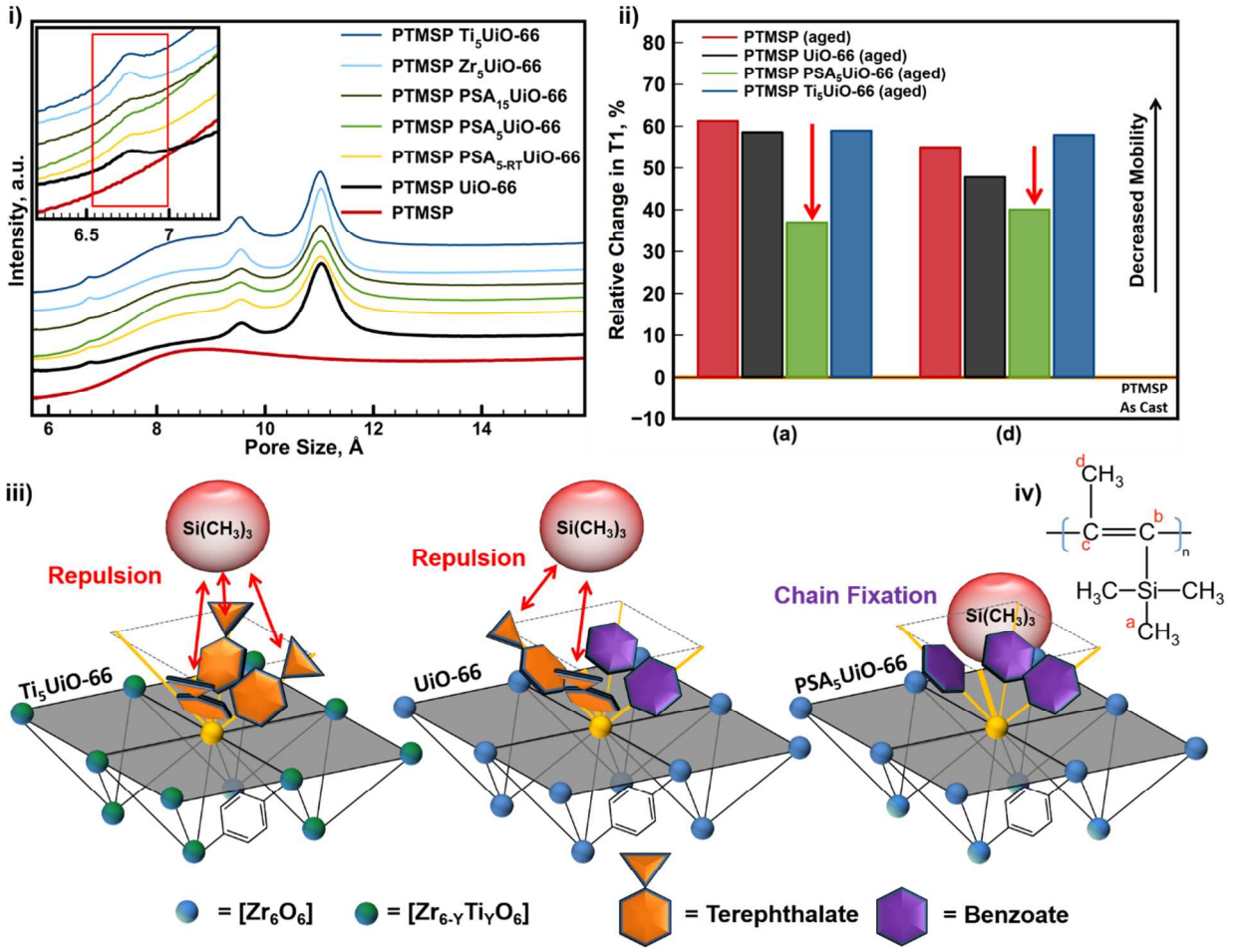


**Figure 5. i)** Small Angle X-ray Scattering patterns of PTMSP and the UiO-66 derived MOF nanocomposites. Insert highlights a scattering peak associated to interfacial free volume most prevalent in films containing $Ti_5UiO$-66, $Zr_5UiO$-66 and UiO-66. **ii)** Relative change in $^{13}C$ T1 relaxation times for aged PTMSP's pendant carbons in the pure polymer and in nanocomposites containing $Ti_5UiO$-66, UiO-66, and $PSA_5UiO$-66; as labelled in **Figure 5iv**. T1 relaxation times for each carbon in "as cast" PTMSP is represented by the yellow horizontal line at 0%. Red arrows highlight the reduced aging effect caused by inclusion of $PSA_5UiO$-66 in PTMSP. All films aged 1 month in ambient conditions. Changes to T1 relaxation times of carbons (b and c) are shown in **Figure S8**, Supporting Information. **iii)** Proposed distribution of terephthalate and

benzoate linkers on the crystal surface of $Ti_5$UiO-66, UiO-66 and $PSA_5$UiO-66 MOFs according to the findings presented. MOF bound hydroxyl groups and DMF, as well as species coordinated to adjacent metal centres have been omitted for clarity. **iv)** Structure of PTMSP with unique carbons labelled a-d, assigned from $^{13}$C NMR chemical shifts: a = 3ppm, b = 151 ppm, c = 138ppm, and d = 26 ppm.

The lesser effect observed here can be explained by the polarity and relative size of the MOF's $Zr_6O_6$ nodes, which repel the hydrophobic polymer and hold terminal aromatic rings further apart than PAF-1's quaternary carbon, preventing chelation between adjacent exposed benzenes of surface benzoate groups and the polymer's trimethylsilyl groups. Interestingly, PTMSP's carbon (b) is almost unchanged after aging in the presence of $Ti_5$UiO-66, supporting our previous findings that suggest a $Ti^{IV}$-alkene interaction (**Figure S8**).[32] These observations support our characterization of the MOF and provide further evidence of the described PSA linker rearrangement. Surface coordinated benzoate (exposed benzene ring) can interact with the polymer methyl groups, whereas the free carboxylic acid and $Ti^{IV}$/$Zr^{IV}$-bound OH groups on the surface of UiO-66 and $Ti_5$UiO-66 instead repel the polymer and cause accelerated aging (**Figure 5iii**).[32] Together, these findings confirm the solvothermal rearrangement of UiO-66's constituent linkers toward a surface-selective capped MOF structure, a class of surface-modified MOFs recently reviewed by McGuire and Forgan.[65] We term this phenomenon 'Post-Synthetic Annealing' (PSA), a previously unreported PSM technique for Metal Organic Frameworks.[11-13]

**MOF-Solution Equilibria Mechanism.** Cohen *et. al.*,[14] showed that in mild solvothermal conditions, MOFs form an equilibrium between framework coordinated and solvated linkers,

without complete dissolution or recrystallization of the parent MOF/s.[13-14] Although some linkers are invariably lost to the solution, this dynamic linker occupancy results in 'active' missing linker sites that can then react with metal ions or re-coordinate to linkers in solution, explaining reported metal/linker substitution[13-15, 19, 28-30, 32, 46] and cluster metalation[19-21, 28] in UiO-66 frameworks. Here, we demonstrate that post-synthetic exchange is influenced by the solvothermal reaction conditions used and has a number of secondary effects on the molecular composition of a modulated UiO-66 framework. In PSE reactions without an exchangeable reagent, described here as Post-Synthetic Annealing, linker mobility allows the mixture of coordinated species to rearrange toward a more thermodynamically stable state.[14] Singly bound terephthalate in the UiO-66 framework are preferentially dissociated into solution, allowing them to migrate to linker defects sites where they are stabilized by the framework. Conversely, as benzoate is not stabilized by missing linker sites between metal clusters within the framework, dissociated benzoate instead favors accumulating on the MOF's outer surfaces. This redistribution of the linker species is supported by the differences in the reaction equilibrium constants for benzoic acid derivatives (**Figure 6**).[66-68] Hammett sigma ($\sigma_p$) constants represent the effect substituent groups at the *meta* or *para* position has on the reactivity of a benzoic acid derivative, relative to benzoic acid for a given reaction. Positive sigma values indicate electron-withdrawing effects that weaken the carboxylate ionic bond, improving the stability of anion; whereas electron-donating groups are expected to cause stronger binding to the MOF nodes. By this perspective, non-bonding COOH groups on the terminal terephthalate (i.e. singly coordinated linkers) weakens these linkers' coordination to UiO-66 nodes causing it to be preferentially removed. Consequently, benzoate's relatively higher stability in this bonding environment causes it to concentrate on the crystal surface. Together, this rearrangement results

in the significant change in polymer interaction observed with the $PSA_xUiO$-66 MOFs. Dissolved linkers may bind to defect sites within the framework, however as the proportion of surface to core linkers is low, these changes to the missing linker concentration would not be easily observed.

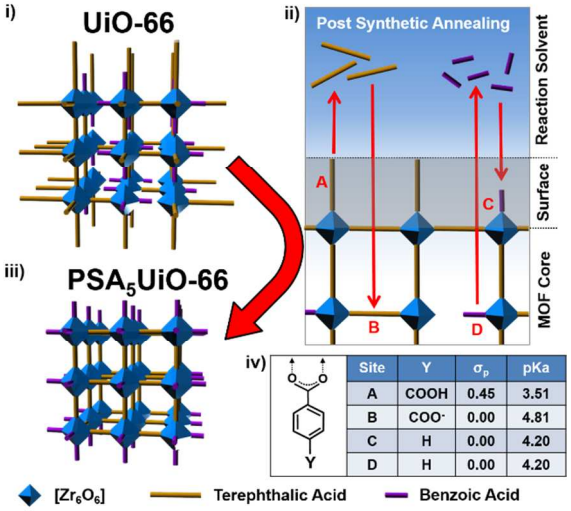


**Figure 6. i)** Single crystal of UiO-66 showing both terephthalate and benzoate linkers in both surface and core positions. **ii)** During Post-Synthetic Annealing, terephthalate and benzoate form an equilibrium with solution that allows linker rearrangement according to the relative stability of their coordination. Letters identify the different bonding environments in UiO-66: **(A)** terephthalate as $[H\text{-}BDC]^-$, singly coordinated at the MOF surface and missing SBU sites (Y = COOH); **(B)** terephthalate as $[BDC]^{2-}$, bridging $Zr_6O_6$ SBUs ($Y = COO^-$); **(C)** benzoate bound to the MOF crystal surface (Y = H); **(D)** benzoate coordinated at a missing linker site (Y = H). Red arrows show the preferred direction of each equilibrium as discussed. **iii)** Single crystal of $PSA_5UiO$-66, highlighting the rearrangement of surface and core linkers. **iv)** Table details the Hammett $\sigma_p$ values corresponding to each benzoic acid derivative species present within the UiO-66 framework and PSA reaction mixture.[66-67]

When metal ions are present, such as $Ti^{IV}$ for the transmetalation of UiO-66 to $Ti_5$UiO-66, results from FTIR and TGA-MS indicate that coordinated benzoate is instead entirely removed from the framework during exchange. Almost identical behavior is observed in the equivalent $Zr^{IV}$ exchanged MOF, despite the absence of a driving force for Zr-Zr metal exchange. Upon dissolution, metal ions react with singly bound terephthalate linkers to form salts that reduce the species' $\sigma_p$ (Ar-COOH = 0.45; Ar-$COO^-$ = 0.00) and stabilizes their attachment to the crystal surface. Benzoate is not stabilized by this mechanism, and due to the large excess of metal cations in solution, dissociated benzoate is effectively sequestered from the MOF by the coordination equilibria with dissolved metal ions. This removal explains the absence of the benzoate in $Ti_5$UiO-66 and $Zr_5$UiO-66 and why these frameworks exhibit considerably higher level of missing linker defects, exposed metal sites, and enhanced gas capacity.[15, 30, 53] Unexpectedly, the similarity of $Zr_5$UiO-66 and $Ti_5$UiO-66 suggests that excess metal ions in solution - rather than specific metal – has a considerable influence over the properties of transmetalated MOFs. Analogous to the discussed linker 'stability', the sigma values ($\sigma_p$) of benzoic acid derivatives also helps explain the synthetic modulation of UiO-66, whereby the competing equilibria present during synthesis moderates crystal growth over the nucleation of new MOF crystals.[14, 39, 46, 49, 69] The chelating effect of bridged terephthalate enables framework propagation, despite the large molar excess of a non-bridging linkers in the reaction mixture. The effect of functional groups on the relative binding strengths of benzoic acid based linkers was further confirmed by UiO-66 prepared using *p*-hydroxybenzoic acid ($\sigma_p$ (OH) = -0.37) as a synthesis modulator, instead of benzoic acid ($\sigma_p$ (H) = 0).[66-67] The resulting amorphous MOF, denoted here as UiO-BzOH, exhibited a similar thermal stability to UiO-66 (**Figures S1ii and S5ii**). As predicted by the Hammett sigma values, *p*-hydroxybenzoic acid competes with

terephthalic acid for $Zr^{IV}$ coordination during MOF assembly, where the preference for the non-bridging linker prevents the formation of a crystalline framework.[39] Based on these findings, the presented mechanism provides a viable explanation for the observed changes to linker and metal species in modified UiO-66 materials.[13-15, 19, 28-30, 32, 46]

## CONCLUSIONS

Here we examine the effect of reaction conditions of Post-Synthetic Modification on the composition and distribution of linker species in UiO-66. Like previous studies that compared different synthesis conditions, it was found that linkers (both bridging and non-bridging) and solvent system chemistry has a considerable effect on the resulting framework. Through this study, we demonstrate the ability to post-synthetically anneal metal organic frameworks, a new PSM technique, as a method of controlling a MOF's surface chemistry. In the absence of an exchangeable species, the non-bridging linker migrated to the particle surface that changed the MOF's interaction with, and the aging of, a well-known glassy polymer. We propose an explanation for these effects through the Hammett constants for reaction rates of benzoic acid based molecules, finding good agreement with both the studied UiO-66 MOFs and a previously unreported but related MOF, UiO-BzOH. Interestingly the other control material, a homo-metal exchanged UiO-66 ($Zr_5$UiO-66), was found to be an unusually good analogue for Ti exchanged UiO-66, providing insight into the root causes of $Ti_5$UiO-66's performance and interaction in super glassy polymer membranes. Given the exponential growth of the MOF field and broad applicability of MOF materials in recent years, a study of the Hammett substituent constants using other carboxylic acid based linkers, as well as binding strength of other MOF species, may hold considerable value to MOF syntheses, PSM, and coordination chemistry in general.

Additionally through our experiments with PTMSP, we demonstrate that PSA is a valuable tool in fine-tuning the interfacial interactions between polymers and MOFs in mixed matrix membranes and should aid the development of advanced MMM materials for industrial separations.

## EXPERIMENTAL METHODS

Langmuir and BET Surface areas measurements were made using a Micromeritic ASAP2040 with liquid $N_2$ (77 K). Powder X-ray diffraction patterns (PXRD) were recorded on a Bruker D8 Advance X-ray Diffractometer, using Cu K-alpha radiation (40kV, 40mA), scanned over the 2-Theta (2θ) range 5° to 85° (step size 0.02°, 0.4 seconds per step) using a LynxEye silicon strip detector. MOF and polymer nanocomposite samples were studied using the Small/Wide Angle X-ray Scattering Beamline at the Australian Synchrotron, Victoria, Australia. Raw data was averaged from four repeat scans between 0.18 - 1.12 and 0.95 - 3.17 using the SAXS and WAXS detectors, respectively. Background scattering (air or Kapton tape) was subtracted from sample data before normalizing to the range q = 0.50-0.55. Simultaneous Thermal Analysis (TGA/DSC) was carried out using a Netzsch STA 449 F1 Jupiter with SiC furnace and S-type sensor. A coupled Pfeiffer Thermostar was used for Evolved Gas Analysis (EGA) by mass spectroscopy. An AXIS Ultra DLD spectrometer (Kratos Analytical Inc., Manchester, UK) with a mono-chromated Al K-alpha source at a power of 144 W (12 kV × 12 mA) fitted with a custom-built shallow well sample holder was used for X-ray Photoelectron Spectroscopy. High resolution spectra were recorded from individual peaks at 40 eV pass energy, with typical pressures of 8-10 mbar in the main chamber during analysis. Data was processed using CasaXPS processing

software version 2.3.15 (Casa Software Ltd., Teignmouth, UK). ICP-OES spectra were collected using an Agilent 730 Series, after lithium borate fusion and digestion. Solid state ($^{13}C$) NMR of MOF samples was measured using a Bruker Av500, spinning speed 13 kHz. T1 relaxation rate constants were calculated from the decay of peak intensity with time of PTMSP carbons in $^{13}C$ NMR spectra in prepared polymer nanocomposites. Fourier-Transform Infrared (FTIR) spectra were collected using a Thermo Scientific NICOLET 6700 FT-IR. Polymer mixed matrix membranes were prepared by solution casting of 10 wt. % loading. Gas permeation ($H_2$, $N_2$, $CO_2$) were measured in duplicate using a custom fixed volume permeation rig used previously. Further details are included in the Supporting Information.

AUTHOR INFORMATION

**Corresponding Author**

* (S.J.D.S.) E-mail: stefan.smith@csiro.au

* (M.R.H.) E-mail: matthew.hill@csiro.au

**Author Contributions**

The manuscript was written through contributions of all authors. All authors have given approval to the final version of the manuscript.

ACKNOWLEDGMENT

This research as supported by the Science and Industry Endowment Fund (SIEF). S.J.D.S. acknowledges support from the Monash University Postgraduate Publications Award. The Authors thank John Burton for inspiring discussion, and Muayad Al-Shaeli for assistance with synthesis of UiO-BzOH. The Authors also thank Marta Rubio Martinez for conducting some of the surface area experiments and Chris Sheedy for the ICP-OES analysis. Parts of this research were undertaken at the Australian Synchrotron, Victoria, Australia. MRH acknowledges FT 1300345.

ASSOCIATED CONTENT

**Supporting Information Available**. Synthesis and Post-synthetic Modification methods, XRD, Surface Area, TGA, NMR, XPS, FTIR, and ICP-OES of the reported MOFs. Nanocomposite preparation, SAXS/WAXS, T1 NMR relaxation, and membrane permselectivty data. (PDF). This information is available free of charge via the Internet at http://pubs.acs.org/.

ABBREVIATIONS

MOF, Metal-Organic Framework; PSM, Post-Synthetic Modification; PSE, Post-Synthetic Exchange; PSA, Post-Synthetic Annealing; SALE, Solvent-Assisted Linker Exchange; MMM, Mixed Matrix Membrane; SBU, Secondary Building Unit (of a MOF).

REFERENCES

1. Tanh Jeazet, H. B.; Staudt, C.; Janiak, C., Metal-Organic Frameworks in Mixed-Matrix Membranes for Gas Separation. *Dalton Trans.* **2012,** *41* (46), 14003-14027.
2. Mason, J. A.; Sumida, K.; Herm, Z. R.; Krishna, R.; Long, J. R., Evaluating metal-organic frameworks for post-combustion carbon dioxide capture via temperature swing adsorption. *Energ. Environ. Sci.* **2011,** *4* (8), 3030-3040.
3. Liu, Y.; Wang, Z. U.; Zhou, H.-C., Recent advances in carbon dioxide capture with metal-organic frameworks. *Greenhouse Gases: Science and Technology* **2012,** *2* (4), 239-259.
4. Liu, J.; Thallapally, P. K.; McGrail, B. P.; Brown, D. R.; Liu, J., Progress in adsorption-based CO2 capture by metal-organic frameworks. *Chem. Soc. Rev.* **2012,** *41* (6), 2308-2322.
5. Zhang, Z.; Yao, Z.-Z.; Xiang, S.; Chen, B., Perspective of microporous metal-organic frameworks for CO2 capture and separation. *Energ. Environ. Sci.* **2014,** *7* (9), 2868-2899.
6. Seoane, B.; Coronas, J.; Gascon, I.; Etxeberria Benavides, M.; Karvan, O.; Caro, J.; Kapteijn, F.; Gascon, J., Metal-organic framework based mixed matrix membranes: a solution for highly efficient CO2 capture? *Chem. Soc. Rev.* **2015,** *44* (8), 2421-54.
7. Zornoza, B.; Tellez, C.; Coronas, J.; Gascon, J.; Kapteijn, F., Metal Organic Framework based Mixed Matrix Membranes: An Increasingly Important Field of Research with a Large Application Potential. *Microporous Mesoporous Mater.* **2013,** *166* (0), 67-78.
8. Evans, J. D.; Sumby, C. J.; Doonan, C. J., Post-synthetic metalation of metal-organic frameworks. *Chem. Soc. Rev.* **2014,** *43* (16), 5933-5951.
9. Xia, W.; Mahmood, A.; Zou, R.; Xu, Q., Metal-organic frameworks and their derived nanostructures for electrochemical energy storage and conversion. *Energ. Environ. Sci.* **2015,** *8* (7), 1837-1866.
10. Cohen, S. M., The Postsynthetic Renaissance in Porous Solids. *J. Am. Chem. Soc.* **2017**.
11. Wang, Z.; Cohen, S. M., Postsynthetic modification of metal-organic frameworks. *Chem. Soc. Rev.* **2009,** *38* (5), 1315-1329.
12. Deria, P.; Mondloch, J. E.; Karagiaridi, O.; Bury, W.; Hupp, J. T.; Farha, O. K., Beyond post-synthesis modification: evolution of metal-organic frameworks via building block replacement. *Chem. Soc. Rev.* **2014,** *43* (16), 5896-5912.
13. Marshall, R. J.; Forgan, R. S., Postsynthetic Modification of Zirconium Metal-Organic Frameworks. *Eur. J. Inorg. Chem.* **2016,** (27), 4310-4331.

14. Kim, M.; Cahill, J. F.; Fei, H.; Prather, K. A.; Cohen, S. M., Postsynthetic Ligand and Cation Exchange in Robust Metal-Organic Frameworks. *J. Am. Chem. Soc.* **2012,** *134* (43), 18082-8.
15. Lau, C. H.; Babarao, R.; Hill, M. R., A Route to Drastic Increase of CO2 Uptake in Zr Metal Organic Framework UiO-66. *Chem. Commun.* **2013,** *49* (35), 3634-3636.
16. Brozek, C. K.; Dinca, M., Cation exchange at the secondary building units of metal-organic frameworks. *Chem. Soc. Rev.* **2014,** *43* (16), 5456-5467.
17. Takaishi, S.; DeMarco, E. J.; Pellin, M. J.; Farha, O. K.; Hupp, J. T., Solvent-assisted linker exchange (SALE) and post-assembly metallation in porphyrinic metal-organic framework materials. *Chem. Sci.* **2013,** *4* (4), 1509-1513.
18. Liu, C.; Luo, T.-Y.; Feura, E. S.; Zhang, C.; Rosi, N. L., Orthogonal Ternary Functionalization of a Mesoporous Metal–Organic Framework via Sequential Postsynthetic Ligand Exchange. *J. Am. Chem. Soc.* **2015,** *137* (33), 10508-10511.
19. Yuan, S.; Chen, Y.-P.; Qin, J.; Lu, W.; Wang, X.; Zhang, Q.; Bosch, M.; Liu, T.-F.; Lian, X.; Zhou, H.-C., Cooperative Cluster Metalation and Ligand Migration in Zirconium Metal–Organic Frameworks. *Angew. Chem. Int. Ed.* **2015,** *54* (49), 14696-14700.
20. Nguyen, H. G. T.; Mao, L.; Peters, A. W.; Audu, C. O.; Brown, Z. J.; Farha, O. K.; Hupp, J. T.; Nguyen, S. T., Comparative study of titanium-functionalized UiO-66: support effect on the oxidation of cyclohexene using hydrogen peroxide. *Catalysis Science & Technology* **2015,** *5* (9), 4444-4451.
21. Nguyen, H. G. T.; Schweitzer, N. M.; Chang, C.-Y.; Drake, T. L.; So, M. C.; Stair, P. C.; Farha, O. K.; Hupp, J. T.; Nguyen, S. T., Vanadium-Node-Functionalized UiO-66: A Thermally Stable MOF-Supported Catalyst for the Gas-Phase Oxidative Dehydrogenation of Cyclohexene. *ACS Catalysis* **2014,** *4* (8), 2496-2500.
22. Kim, M.; Cohen, S. M., Discovery, development, and functionalization of Zr(iv)-based metal-organic frameworks. *CrystEngComm* **2012,** *14* (12), 4096-4104.
23. Shultz, A. M.; Sarjeant, A. A.; Farha, O. K.; Hupp, J. T.; Nguyen, S. T., Post-Synthesis Modification of a Metal–Organic Framework To Form Metallosalen-Containing MOF Materials. *J. Am. Chem. Soc.* **2011,** *133* (34), 13252-13255.
24. Zhang, Y.; Feng, X.; Li, H.; Chen, Y.; Zhao, J.; Wang, S.; Wang, L.; Wang, B., Photoinduced Postsynthetic Polymerization of a Metal–Organic Framework toward a Flexible Stand-Alone Membrane. *Angew. Chem. Int. Ed.* **2015,** *54* (14), 4259-4263.
25. Shalini, S.; Dhavale, V. M.; Eldho, K. M.; Kurungot, S.; Ajithkumar, T. G.; Vaidhyanathan, R., 1000-fold enhancement in proton conductivity of a MOF using post-synthetically anchored proton transporters. *Scientific Reports* **2016,** *6*, 32489.
26. Phang, W. J.; Jo, H.; Lee, W. R.; Song, J. H.; Yoo, K.; Kim, B.; Hong, C. S., Superprotonic Conductivity of a UiO-66 Framework Functionalized with Sulfonic Acid Groups by Facile Postsynthetic Oxidation. *Angew. Chem. Int. Ed.* **2015,** *54* (17), 5142-5146.
27. Wang, C.; Liu, X.; Chen, J. P.; Li, K., Superior removal of arsenic from water with zirconium metal-organic framework UiO-66. *Scientific Reports* **2015,** *5*, 16613.
28. Nouar, F.; Breeze, M. I.; Campo, B. C.; Vimont, A.; Clet, G.; Daturi, M.; Devic, T.; Walton, R. I.; Serre, C., Tuning the properties of the UiO-66 metal organic framework by Ce substitution. *Chem. Commun.* **2015,** *51* (77), 14458-14461.
29. Navarro Amador, R.; Carboni, M.; Meyer, D., Photosensitive titanium and zirconium Metal Organic Frameworks: Current research and future possibilities. *Mater. Lett.* **2016,** *166*, 327-338.

30. Smith, S. J. D.; Ladewig, B. P.; Hill, A. J.; Lau, C. H.; Hill, M. R., Post-synthetic Ti Exchanged UiO-66 Metal-Organic Frameworks that Deliver Exceptional Gas Permeability in Mixed Matrix Membranes. *Sci. Rep.* **2015,** *5* (7823), 7823.
31. Su, N. C.; Sun, D. T.; Beavers, C. M.; Britt, D. K.; Queen, W. L.; Urban, J. J., Enhanced permeation arising from dual transport pathways in hybrid polymer–MOF membranes. *Energy Environ. Sci.* **2016,** *9* (3), 922-931.
32. Smith, S. J. D.; Lau, C. H.; Mardel, J. I.; Kitchin, M.; Konstas, K.; Ladewig, B. P.; Hill, M. R., Physical aging in glassy mixed matrix membranes; tuning particle interaction for mechanically robust nanocomposite films. *J. Mater. Chem. A* **2016,** *4* (27), 10627-10634.
33. Shen, J.; Liu, G.; Huang, K.; Li, Q.; Guan, K.; Li, Y.; Jin, W., UiO-66-polyether block amide mixed matrix membranes for CO2 separation. *J. Membr. Sci.* **2016,** *513*, 155-165.
34. Jiang, J.-Q.; Yang, C.-X.; Yan, X.-P., Postsynthetic ligand exchange for the synthesis of benzotriazole-containing zeolitic imidazolate framework. *Chem. Commun.* **2015,** *51* (30), 6540-6543.
35. Li, T.; Kozlowski, M. T.; Doud, E. A.; Blakely, M. N.; Rosi, N. L., Stepwise Ligand Exchange for the Preparation of a Family of Mesoporous MOFs. *J. Am. Chem. Soc.* **2013,** *135* (32), 11688-11691.
36. Gadipelli, S.; Guo, Z., Postsynthesis Annealing of MOF-5 Remarkably Enhances the Framework Structural Stability and CO2 Uptake. *Chem. Mater.* **2014,** *26* (22), 6333-6338.
37. Aiyappa, H. B.; Pachfule, P.; Banerjee, R.; Kurungot, S., Porous Carbons from Nonporous MOFs: Influence of Ligand Characteristics on Intrinsic Properties of End Carbon. *Cryst. Growth Des.* **2013,** *13* (10), 4195-4199.
38. Lu, W.; Wei, Z.; Gu, Z.-Y.; Liu, T.-F.; Park, J.; Park, J.; Tian, J.; Zhang, M.; Zhang, Q.; Gentle Iii, T.; Bosch, M.; Zhou, H.-C., Tuning the structure and function of metal-organic frameworks via linker design. *Chem. Soc. Rev.* **2014,** *43* (16), 5561-5593.
39. Ramanan, A.; Whittingham, M. S., How Molecules Turn into Solids: the Case of Self-Assembled Metal−Organic Frameworks. *Cryst. Growth Des.* **2006,** *6* (11), 2419-2421.
40. Fang, Z.; Bueken, B.; De Vos, D. E.; Fischer, R. A., Defect-Engineered Metal–Organic Frameworks. *Angew. Chem. Int. Ed.* **2015,** *54* (25), 7234-7254.
41. St. Petkov, P.; Vayssilov, G. N.; Liu, J.; Shekhah, O.; Wang, Y.; Wöll, C.; Heine, T., Defects in MOFs: A Thorough Characterization. *ChemPhysChem* **2012,** *13* (8), 2025-2029.
42. Ameloot, R.; Vermoortele, F.; Hofkens, J.; De Schryver, F. C.; De Vos, D. E.; Roeffaers, M. B. J., Three-Dimensional Visualization of Defects Formed during the Synthesis of Metal–Organic Frameworks: A Fluorescence Microscopy Study. *Angew. Chem. Int. Ed.* **2013,** *52* (1), 401-405.
43. Chui, S. S.-Y.; Lo, S. M.-F.; Charmant, J. P. H.; Orpen, A. G.; Williams, I. D., A Chemically Functionalizable Nanoporous Material [Cu3(TMA)2(H2O)3]n. *Science* **1999,** *283* (5405), 1148-1150.
44. Li, H.; Eddaoudi, M.; O'Keeffe, M.; Yaghi, O. M., Design and synthesis of an exceptionally stable and highly porous metal-organic framework. *Nature* **1999,** *402* (6759), 276-279.
45. Cavka, J. H.; Jakobsen, S.; Olsbye, U.; Guillou, N.; Lamberti, C.; Bordiga, S.; Lillerud, K. P., A New Zirconium Inorganic Building Brick Forming Metal Organic Frameworks with Exceptional Stability. *J. Am. Chem. Soc.* **2008,** *130* (42), 13850-13851.
46. Wu, H.; Chua, Y. S.; Krungleviciute, V.; Tyagi, M.; Chen, P.; Yildirim, T.; Zhou, W., Unusual and Highly Tunable Missing-Linker Defects in Zirconium Metal–Organic Framework

UiO-66 and Their Important Effects on Gas Adsorption. *J. Am. Chem. Soc.* **2013,** *135* (28), 10525-10532.
47. Hu, Z.; Zhao, D., De facto methodologies toward the synthesis and scale-up production of UiO-66-type metal-organic frameworks and membrane materials. *Dalton Trans.* **2015,** *44* (44), 19018-19040.
48. Cliffe, M. J.; Wan, W.; Zou, X.; Chater, P. A.; Kleppe, A. K.; Tucker, M. G.; Wilhelm, H.; Funnell, N. P.; Coudert, F.-X.; Goodwin, A. L., Correlated Defect Nanoregions in a Metal–Organic Framework. *Nat. Commun.* **2014,** *5*, 4176.
49. Valenzano, L.; Civalleri, B.; Chavan, S.; Bordiga, S.; Nilsen, M. H.; Jakobsen, S.; Lillerud, K. P.; Lamberti, C., Disclosing the Complex Structure of UiO-66 Metal Organic Framework: A Synergic Combination of Experiment and Theory. *Chem. Mater.* **2011,** *23* (7), 1700-1718.
50. Shearer, G. C.; Chavan, S.; Ethiraj, J.; Vitillo, J. G.; Svelle, S.; Olsbye, U.; Lamberti, C.; Bordiga, S.; Lillerud, K. P., Tuned to Perfection: Ironing Out the Defects in Metal–Organic Framework UiO-66. *Chem. Mater.* **2014,** *26* (14), 4068-4071.
51. Hu, Z.; Castano, I.; Wang, S.; Wang, Y.; Peng, Y.; Qian, Y.; Chi, C.; Wang, X.; Zhao, D., Modulator Effects on the Water-Based Synthesis of Zr/Hf Metal–Organic Frameworks: Quantitative Relationship Studies between Modulator, Synthetic Condition, and Performance. *Cryst. Growth Des.* **2016,** *16* (4), 2295-2301.
52. Trickett, C. A.; Gagnon, K. J.; Lee, S.; Gándara, F.; Bürgi, H.-B.; Yaghi, O. M., Definitive Molecular Level Characterization of Defects in UiO-66 Crystals. *Angew. Chem. Int. Ed.* **2015,** *54* (38), 11162-11167.
53. Vermoortele, F.; Bueken, B.; Le Bars, G.; Van de Voorde, B.; Vandichel, M.; Houthoofd, K.; Vimont, A.; Daturi, M.; Waroquier, M.; Van Speybroeck, V.; Kirschhock, C.; De Vos, D. E., Synthesis Modulation as a Tool To Increase the Catalytic Activity of Metal–Organic Frameworks: The Unique Case of UiO-66(Zr). *J. Am. Chem. Soc.* **2013,** *135* (31), 11465-11468.
54. Lau, C. H.; Nguyen, P. T.; Hill, M. R.; Thornton, A. W.; Konstas, K.; Doherty, C. M.; Mulder, R. J.; Bourgeois, L.; Liu, A. C. Y.; Sprouster, D. J.; Sullivan, J. P.; Bastow, T. J.; Hill, A. J.; Gin, D. L.; Noble, R. D., Ending Aging in Super Glassy Polymer Membranes. *Angew. Chem. Int. Ed.* **2014,** *53* (21), 5322-5326.
55. Yampolskii, Y., Polymeric Gas Separation Membranes. *Macromolecules* **2012,** *45* (8), 3298-3311.
56. Aroon, M. A.; Ismail, A. F.; Matsuura, T.; Montazer-Rahmati, M. M., Performance studies of mixed matrix membranes for gas separation: A review. *Sep. Purif. Technol.* **2010,** *75* (3), 229-242.
57. Khdhayyer, M. R.; Esposito, E.; Fuoco, A.; Monteleone, M.; Giorno, L.; Jansen, J. C.; Attfield, M. P.; Budd, P. M., Mixed matrix membranes based on UiO-66 MOFs in the polymer of intrinsic microporosity PIM-1. *Sep. Purif. Technol.* **2017,** *173*, 304-313.
58. Katz, M. J.; Brown, Z. J.; Colon, Y. J.; Siu, P. W.; Scheidt, K. A.; Snurr, R. Q.; Hupp, J. T.; Farha, O. K., A facile synthesis of UiO-66, UiO-67 and their derivatives. *Chem. Commun.* **2013,** *49* (82), 9449-9451.
59. Shearer, G. C.; Chavan, S.; Bordiga, S.; Svelle, S.; Olsbye, U.; Lillerud, K. P., Defect Engineering: Tuning the Porosity and Composition of the Metal–Organic Framework UiO-66 via Modulated Synthesis. *Chem. Mater.* **2016,** *28* (11), 3749-3761.
60. Sabo, M.; Bohlmann, W.; Kaskel, S., Titanium terephthalate (TT-1) hybrid materials with high specific surface area. *J. Mater. Chem.* **2006,** *16* (24), 2354-2357.

61. Kitchin, M.; Teo, J.; Konstas, K.; Lau, C. H.; Sumby, C. J.; Thornton, A. W.; Doonan, C. J.; Hill, M. R., AIMs: a new strategy to control physical aging and gas transport in mixed-matrix membranes. *J. Mater. Chem. A* **2015,** *3* (29), 15241-15247.
62. Lau, C. H.; Konstas, K.; Doherty, C. M.; Kanehashi, S.; Ozcelik, B.; Kentish, S. E.; Hill, A. J.; Hill, M. R., Tailoring Physical Aging in Super Glassy Polymers with Functionalized Porous Aromatic Frameworks for CO2 Capture. *Chem. Mater.* **2015,** *27* (13), 4756-4762.
63. Lau, C. H.; Mulet, X.; Konstas, K.; Doherty, C. M.; Sani, M.-A.; Separovic, F.; Hill, M. R.; Wood, C. D., Hypercrosslinked Additives for Ageless Gas-Separation Membranes. *Angew. Chem. Int. Ed.* **2016,** *55* (6), 1998-2001.
64. Hill, A. J.; Pas, S. J.; Bastow, T. J.; Burgar, M. I.; Nagai, K.; Toy, L. G.; Freeman, B. D., Influence of methanol conditioning and physical aging on carbon spin-lattice relaxation times of poly(1-trimethylsilyl-1-propyne). *J. Membr. Sci.* **2004,** *243* (1–2), 37-44.
65. McGuire, C. V.; Forgan, R. S., The surface chemistry of metal-organic frameworks. *Chem. Commun.* **2015,** *51* (25), 5199-5217.
66. McDaniel, D. H.; Brown, H. C., An Extended Table of Hammett Substitutent Constants Based on the Ionization of Substituted Benzoic Acids. *The Journal of Organic Chemistry* **1958,** *23* (3), 420-427.
67. Hansch, C.; Leo, A.; Taft, R. W., A survey of Hammett substituent constants and resonance and field parameters. *Chem. Rev. (Washington, DC, U. S.)* **1991,** *91* (2), 165-195.
68. Hahm, H.; Yoo, K.; Ha, H.; Kim, M., Aromatic Substituent Effects on the Flexibility of Metal–Organic Frameworks. *Inorg. Chem.* **2016,** *55* (15), 7576-7581.
69. Schaate, A.; Roy, P.; Godt, A.; Lippke, J.; Waltz, F.; Wiebcke, M.; Behrens, P., Modulated Synthesis of Zr-Based Metal–Organic Frameworks: From Nano to Single Crystals. *Chem. Eur. J.* **2011,** *17* (24), 6643-6651.

FOR TABLE OF CONTENTS USE ONLY

**Post-Synthetic Annealing: Linker Self-Exchange in UiO-66 and its Effect on Polymer-MOF Interaction**

Stefan J. D. Smith,* † ‡ Kristina Konstas† Cher Hon Lau,†§ Yesim M. Gozukara,† Christopher D. Easton,† Roger J. Mulder,† Bradley P. Ladewig, ‡• and Matthew R. Hill*† ‡

**Annealing MOFs:** Controlled redistribution of bound linker species within a metal organic framework. By solvothermally concentrating the modulator on the surface of UiO-66 crystals, post-synthetic annealing is shown to be as a facile mean of modifying non-perfect MOFs and improving their compatibility in polymer matrices.

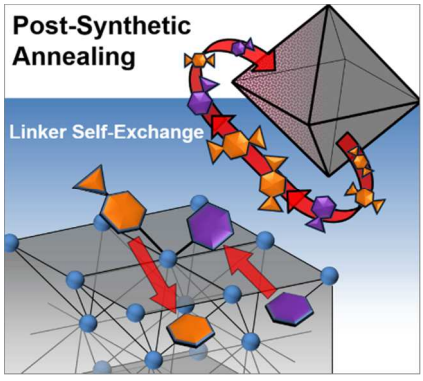

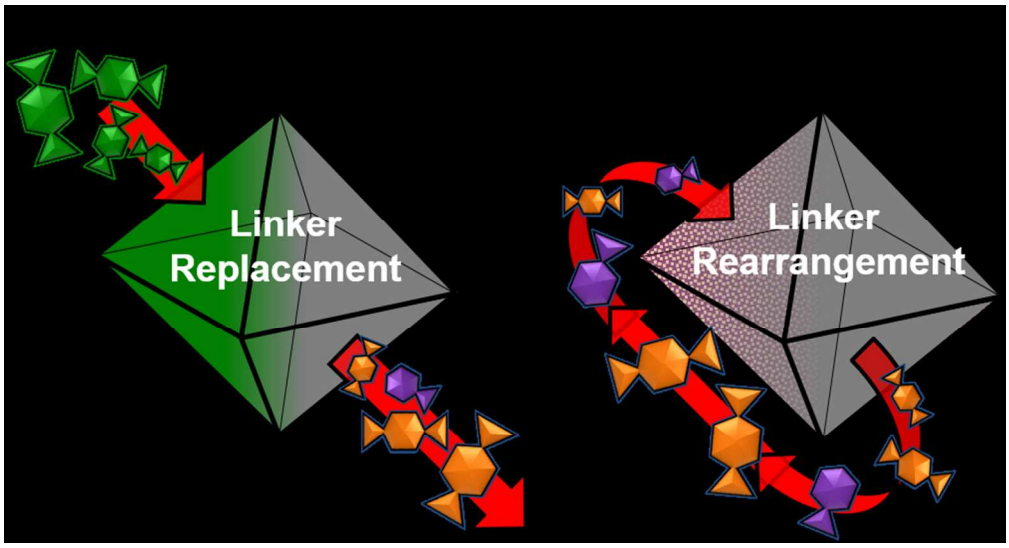


**Figure 1.** General scheme showing how Post-Synthetic Annealing differs from Post-Synthetic Exchange and other Post-Synthetic Modifications.[10]

170x91mm (150 x 150 DPI)

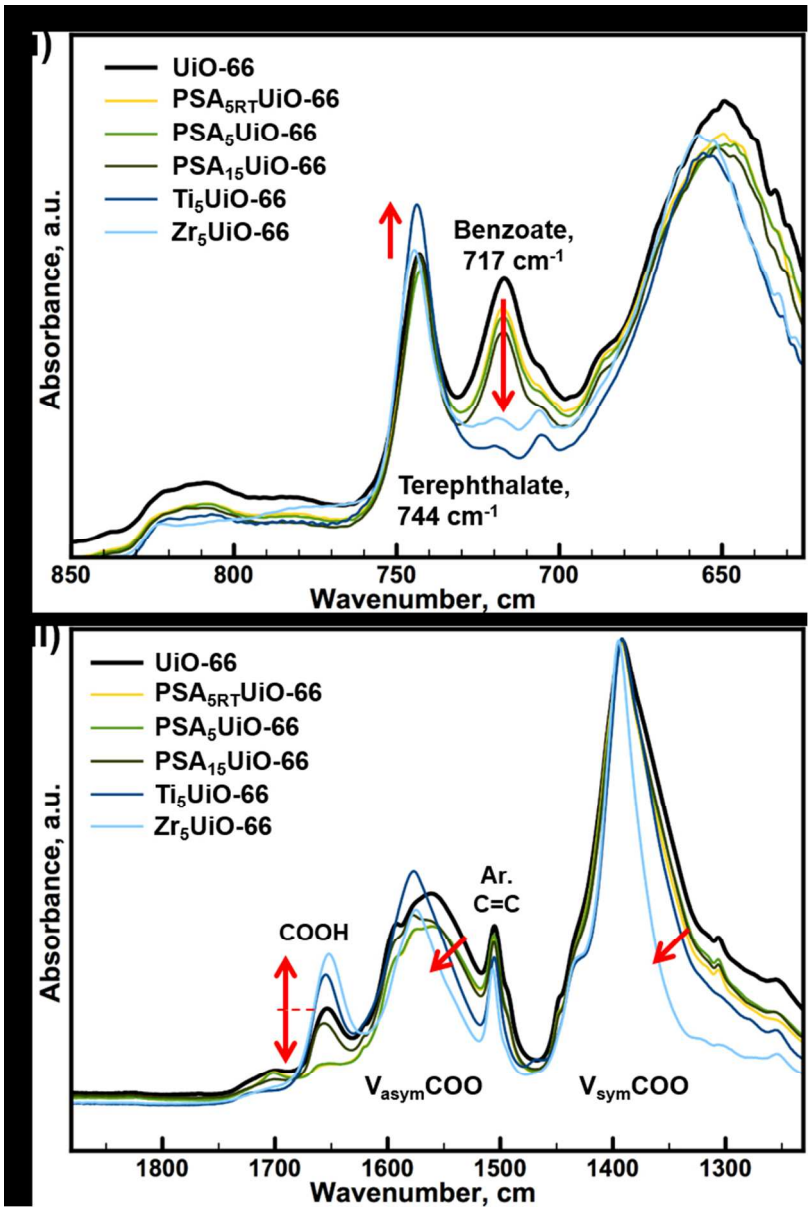


**Figure 2.** Changes to infrared adsorption spectra across the **i)** 600 - 850 $cm^{-1}$ and **ii)** 1200 - 1850 $cm^{-1}$ regions in each of the studied UiO-66 based MOFs, normalised to the peak height of $V_{sym}COO$, 1391 $cm^{-1}$.

132x198mm (150 x 150 DPI)

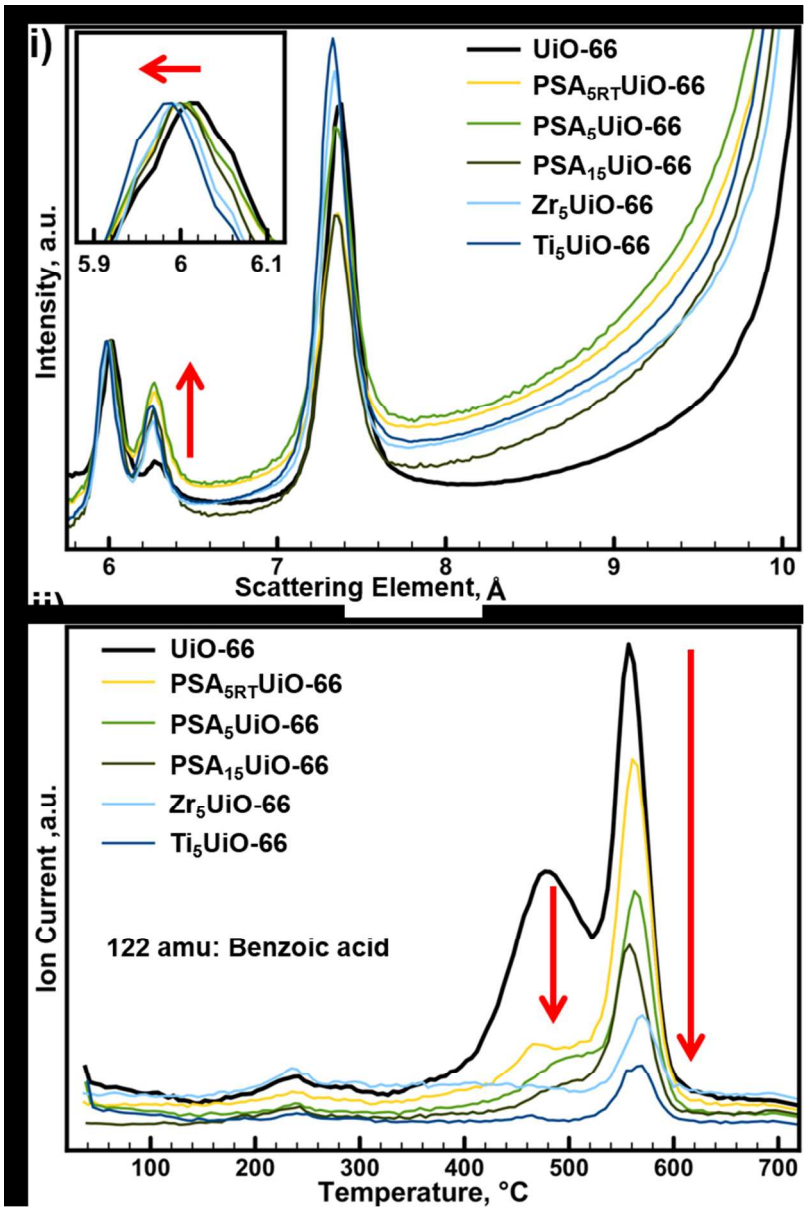


**Figure 3. i)** Small Angle X-ray Scattering patterns, normalized to the ~6 Å peak after subtracting a Kapton background. Red arrows highlight changes to the scattering pattern after PSA or PSE of UiO-66. Insert highlights the discussed reduction in size of scattering elements. **ii)** Mass Spectrometer response from gases evolved during Thermal Gravimetric Analysis of UiO-66 and the exchanged MOFs at 122 amu, associated to benzoic acid/benzoate species. Detected benzoic acid in $Ti_5$UiO-66 and $Zr_5$UiO-66 are explained by the high temperature decomposition of terephthalic acid present in the frameworks. EGA curves for species with masses of 166 amu (terephthalic acid), 78 amu (benzene), and 44 amu (carbon dioxide) are included in the Supporting Information.

127x192mm (150 x 150 DPI)

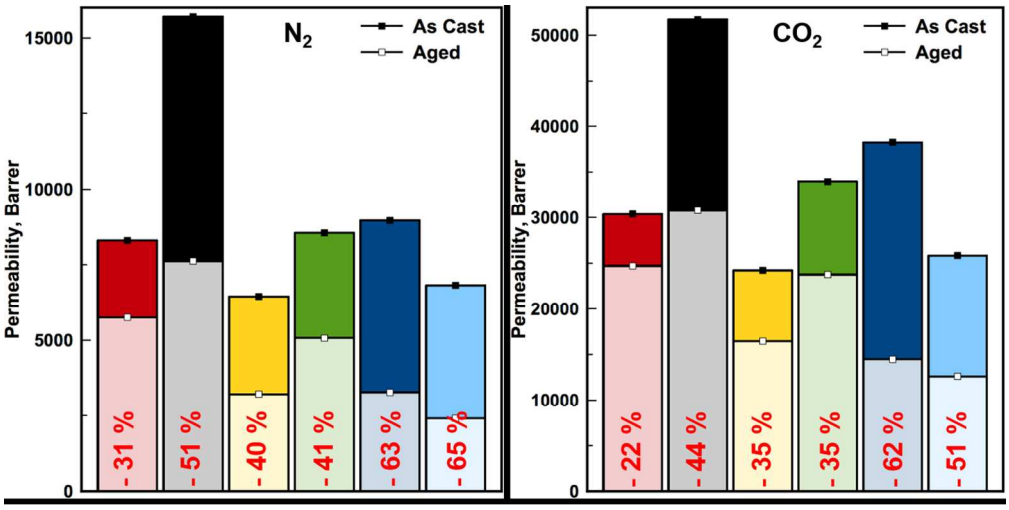


**Figure 4.** Changes in $N_2$ and $CO_2$ Permeability of studied UiO-66 MOFs in PTMSP over time. Samples identified by colour: PTMSP (red), PTMSP nanocomposites with UiO-66 (black), $PSA_{5RT}$UiO-66 (yellow), $PSA_5$UiO-66 (green), $Ti_5$UiO-66 (navy), and $Zr_5$UiO-66 (blue). Films aged for 17 days in ambient conditions. Similar trends are observed for the permeability of $H_2$, see **Figure S7** of the Supporting Information.

239x119mm (150 x 150 DPI)

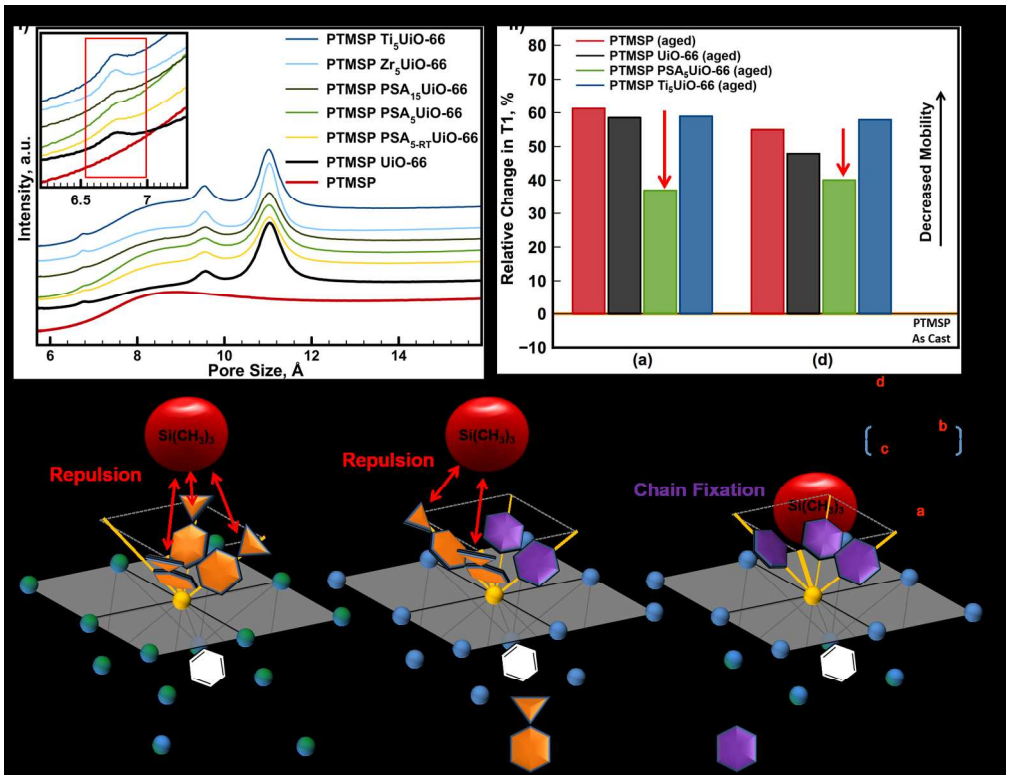


**Figure 5. i)** Small Angle X-ray Scattering patterns of PTMSP and the UiO-66 derived MOF nanocomposites. Insert highlights a scattering peak associated to interfacial free volume most prevalent in films containing $Ti_5$UiO-66, $Zr_5$UiO-66 and UiO-66. **ii)** Relative change in $^{13}C$ T1 relaxation times for aged PTMSP's pendant carbons in the pure polymer and in nanocomposites containing $Ti_5$UiO-66, UiO-66, and $PSA_5$UiO-66; as labelled in **Figure 5iv.** T1 relaxation times for each carbon in "as cast" PTMSP is represented by the yellow horizontal line at 0%. Red arrows highlight the reduced aging effect caused by inclusion of $PSA_5$UiO-66 in PTMSP. All films aged 1 month in ambient conditions. Changes to T1 relaxation times of carbons (b and c) are shown in **Figure S8**, Supporting Information. **iii)** Proposed distribution of terephthalate and benzoate linkers on the crystal surface of $Ti_5$UiO-66, UiO-66 and $PSA_5$UiO-66 MOFs according to the findings presented. MOF bound hydroxyl groups and DMF, as well as species coordinated to adjacent metal centres have been omitted for clarity. **iv)** Structure of PTMSP with unique carbons labelled a-d, assigned from $^{13}C$ NMR chemical shifts: a = 3ppm, b = 151 ppm, c = 138ppm, and d = 26 ppm.

333x255mm (150 x 150 DPI)

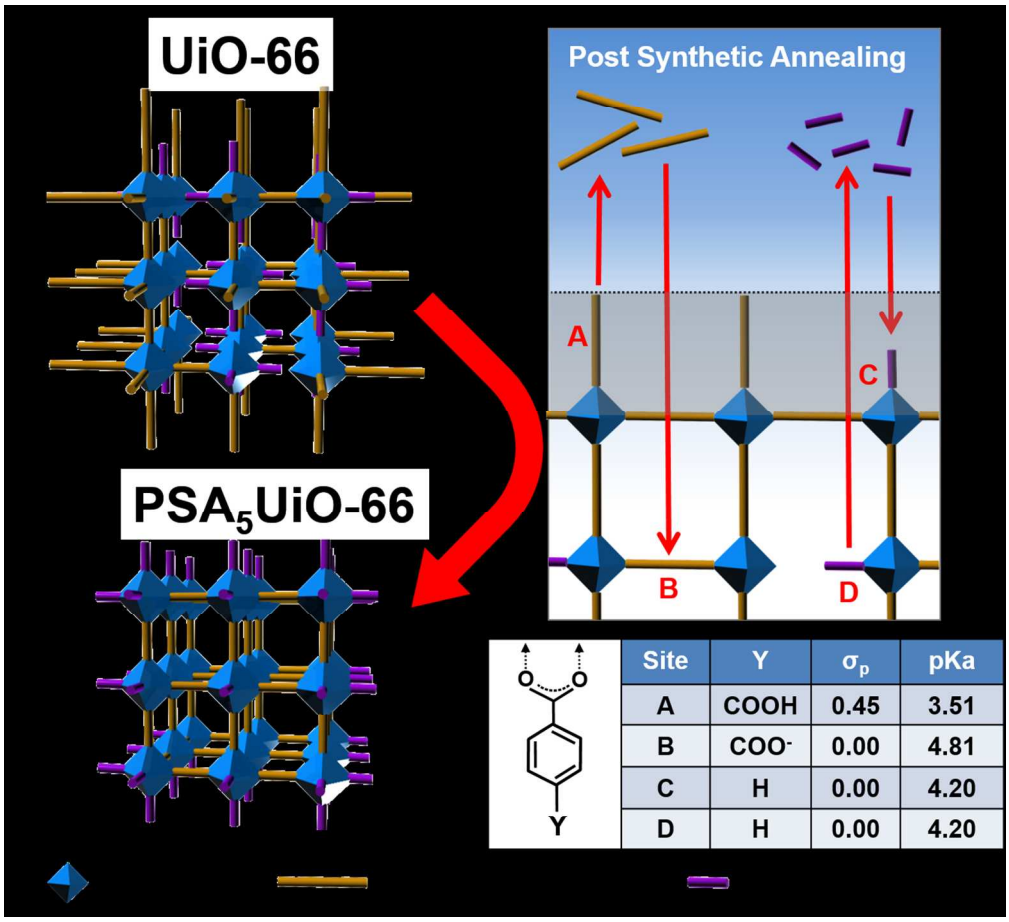


| Site | Y | $\sigma_p$ | pKa |
|---|---|---|---|
| A | COOH | 0.45 | 3.51 |
| B | $COO^-$ | 0.00 | 4.81 |
| C | H | 0.00 | 4.20 |
| D | H | 0.00 | 4.20 |

**Figure 6. i)** Single crystal of UiO-66 showing both terephthalate and benzoate linkers in both surface and core positions. **ii)** During Post-Synthetic Annealing, terephthalate and benzoate form an equilibrium with solution that allows linker rearrangement according to the relative stability their coordination. Letters identify the different bonding environments in UiO-66: **(A)** terephthalate as $[H\text{-}BDC]^-$, singly coordinated at the MOF surface and missing SBU sites (Y = COOH); **(B)** terephthalate as $[BDC]^{2-}$, bridging $Zr_6O_6$ SBUs (Y = $COO^-$); **(C)** benzoate bound to the MOF crystal surface (Y = H); **(D)** benzoate coordinated at a missing linker site (Y = H). Red arrows show the preferred direction of each equilibrium as discussed. **iii)** Single crystal of $PSA_5UiO\text{-}66$, highlighting the rearrangement of surface and core linkers. **iv)** Table details the Hammett $\sigma_p$ values corresponding to each benzoic acid derivative species present within the UiO-66 framework and PSA reaction mixture.[66-67]

226x205mm (150 x 150 DPI)